J Appl Physiol 115: 1402–1414, 2013.
First published August 29, 2013; doi:10.1152/japplphysiol.00762.2013.

Spatiotemporal properties of high-speed calcium oscillations in the pedunculopontine nucleus

James Hyde,[1] Nebojsa Kezunovic,[1] Francisco J. Urbano,[2]* and Edgar Garcia-Rill[1]*

[1]*Center for Translational Neuroscience, Department of Neurobiology & Developmental Sciences, University of Arkansas for Medical Sciences, Little Rock, Arkansas; and* [2]*IFIBYNE, CONICET, University of Buenos Aires, Buenos Aires, Argentina*

Submitted 3 July 2013; accepted in final form 25 August 2013

Hyde J, Kezunovic N, Urbano FJ, Garcia-Rill E. Spatiotemporal properties of high-speed calcium oscillations in the pedunculopontine nucleus. *J Appl Physiol* 115: 1402–1414, 2013. First published August 29, 2013; doi:10.1152/japplphysiol.00762.2013.—The pedunculopontine nucleus (PPN) is a component of the reticular activating system (RAS), and is involved in the activated states of waking and rapid eye movement (REM) sleep. Gamma oscillations (approximately 30–80 Hz) are evident in all PPN neurons and are mediated by high-threshold voltage-dependent N- and P/Q-type calcium channels. We tested the hypothesis that high-speed calcium imaging would reveal calcium-mediated oscillations in dendritic compartments in synchrony with patch-clamp recorded oscillations during depolarizing current ramps. Patch-clamped 8- to 16-day-old rat PPN neurons (n = 67 out of 121) were filled with Fura 2, Bis Fura, or OGB1/CHR. This study also characterized a novel ratiometric technique using Oregon Green BAPTA-1 (OGB1) with coinjections of a new long-stokes-shift dye, Chromeo 494 (CHR). Fluorescent calcium transients were blocked with the nonspecific calcium channel blocker cadmium, or by the combination of ω-agatoxin-IVA, a specific P/Q-type calcium channel blocker, and ω-conotoxin-GVIA, a specific N-type calcium channel blocker. The calcium transients were evident in different dendrites (suggesting channels are present throughout the dendritic tree) along the sampled length without interruption (suggesting channels are evenly distributed), and appeared to represent a summation of oscillations present in the soma. We confirm that PPN calcium channel-mediated oscillations are due to P/Q- and N-type channels, and reveal that these channels are distributed along the dendrites of PPN cells.

arousal; calcium imaging; P/Q channels

THE PEDUNCULOPONTINE NUCLEUS (PPN) is the cholinergic arm of the reticular activating system (38). The PPN is active mainly during the states of waking and paradoxical sleep, and sends ascending projections to the thalamus, especially the parafascicular nucleus (Pf), and descending projections to the pons and medulla (8). Cortical electroencephalograms are characterized by low-amplitude, high-frequency oscillatory activity in the gamma band range (approximately 30–100 Hz) during waking and rapid eye movement (REM) sleep. These gamma oscillations have been proposed to participate in sensory perception, problem solving, memory, and REM sleep (7, 12, 27, 29, 43). These oscillations are believed to participate in thalamocortical processes, where they may participate in the binding or unification of sensory information arising from different cortical regions (24). We recently showed the presence of gamma band (30–80 Hz) oscillatory activity in both PPN and Pf nuclei (20, 21). The rising phase of these oscillations are mediated by high-threshold, voltage-dependent P/Q-type ($Ca_v2.1$) and N-type ($Ca_v2.2$) calcium channels. The falling phase of each oscillation is mediated by potassium channels (K_v 1.1, K_v 1.2, K_v 1.6) (21). Interestingly, P/Q-type knockout mice demonstrate a dramatic reduction in gamma band activity in in vivo recordings. This model also manifests neurological problems such as disrupted sleep-wake cycles, difficulty waking, absence seizures, ataxia, and dystonia near postnatal day 10 (18). The symptoms progress until the mice are unable to walk, and subsequently die at ~3 wk of age (23). These channels have been localized to the dendrites in thalamocortical neurons using calcium imaging (28). We recently described the spatiotemporal properties of calcium oscillations in both the soma and proximal dendrites of Pf neurons using high-speed calcium imaging (14). Knowing the channel location is particularly useful in understanding why these cells need to be highly depolarized to activate the P/Q-type calcium channels. Because dendrites represent high-resistance pathways, higher depolarizing potentials (applied at the soma) are necessary to only partially depolarize the distal dendrites. If P/Q-type and N-type channels are more distal in the dendrite, higher depolarizing currents must be injected into the soma to activate them. The present study was undertaken to determine the spatiotemporal properties of high-threshold calcium channel-dependent membrane oscillations in the dendrites of PPN neurons using calcium imaging.

The PPN is composed of mostly nonoverlapping populations of cholinergic, glutamatergic, and GABAergic neurons (44). In vivo extracellular recordings characterized six categories of thalamic-projecting PPN neurons distinguished by their firing properties relative to ponto-geniculo-occipital wave generation (39). Some of these neurons exhibited low rates of firing (<10 Hz), but the majority had high rates of tonic firing (20–80 Hz). PPN neurons have been shown to increase firing during either REM sleep (REM-on) or REM sleep and waking (wake/REM-on). These cells also show decreased firing during slow-wave sleep (5, 33, 39). Furthermore, injections of glutamate into the PPN increased waking and paradoxical sleep (6), whereas injections of the glutamatergic receptor agonist *N*-methyl-D-aspartic acid (NMDA) increased only waking (4). Injections of kainic acid increased only paradoxical sleep (5). These experiments suggest that the PPN plays a major role in sleep regulation in vivo. In vitro studies of PPN neurons describe three PPN cell types on the basis of their intrinsic properties. Type I neurons possess low-threshold spikes (LTS), whereas type II neurons have an A current. Type III neurons have both A and LTS (22). Other studies showed that two-thirds of type II neurons were cholinergic, whereas one-third of type III neurons were cholinergic (41). Although in vitro studies have

* F. J. Urbano and E. Garcia-Rill contributed equally to this work.

Address for reprint requests and other correspondence: E. Garcia-Rill, Director, Center for Translational Neuroscience, Univ. of Arkansas for Medical Sciences, 4301 W. Markham St., Slot 847, Little Rock, AR 72205 (e-mail: GarciarillEdgar@uams.edu).

shown that all PPN cells fired maximally at gamma band frequencies (21), we do not know where the calcium channels responsible for manifesting gamma band activity are located.

These studies characterized the spatial distribution of beta/gamma band oscillations in PPN neurons using traditional ratiometric calcium probes and a novel ratiometric imaging technique. We studied both P/Q- and N-type calcium channel-mediated oscillations in PPN neurons with the goal of determining the calcium transient properties generated by these two channel types. Our results provide a direct correlation between electrophysiologically determined membrane potential beta/gamma band oscillations and intracellular calcium levels. Our results suggest that these channels are located throughout the dendritic tree and that beta/gamma oscillations may play a major role in second messenger pathways throughout the intracellular compartments of PPN neurons.

MATERIALS AND METHODS

Slice preparation. All experimental protocols were approved by the Institutional Animal Care and Use Committee of the University of Arkansas for Medical Sciences and were in agreement with the National Institutes of Health *Guidelines for the Care and Use of Laboratory Animals*. Rat pups aged 8–16 days were taken from adult timed-pregnant Sprague-Dawley dams. Pups were anesthetized with ketamine (70 mg/kg, i.m.) until the tail pinch reflex was absent. Pups were decapitated and the brain was rapidly removed and cooled in oxygenated sucrose-artificial cerebrospinal fluid (sucrose-aCSF). The sucrose-aCSF consisted of (in mM) sucrose, 233.7; $NaHCO_3$, 26; KCl, 3; $MgCl_2$, 8; $CaCl_2$, 0.5; glucose, 20; ascorbic acid, 0.4; and sodium pyruvate, 2. Sagittal sections (400 μm) containing the PPN nucleus were cut under cooled oxygenated sucrose-aCSF with a Leica VT1200S vibratome (Leica Biosystems, Buffalo Grove, IL) with a minichiller (Huber, Offenburg, Germany), and allowed to equilibrate in normal aCSF at room temperature for 1 h. The aCSF was composed of (in mM) NaCl, 117; KCl, 4.7; $MgCl_2$, 1.2; $CaCl_2$, 2.5; NaH_2PO_4, 1.2; $NaHCO_3$, 24.9; and glucose, 11.5. Slices were recorded at 37°C while being superfused (1.5 ml/min) with oxygenated (95% O_2 and 5% CO_2) aCSF in an immersion chamber. The aCSF contained the following synaptic receptor antagonists: the selective NMDA receptor antagonist 2-amino-5-phosphonovaleric acid (40 μM); the competitive AMPA/kainate glutamate receptor antagonist 6-cyano-7nitroquinox-aline-2,3-dione (1 μM); the glycine receptor antagonist strychnine (10 μM); and the specific $GABA_A$ receptor antagonist gabazine (10 μM).

Whole-cell patch-clamp recordings. An infrared differential interference contrast optics technique was used to visualize neurons using an upright microscope (Nikon FN-1) and QICAM camera (QImaging, Surrey, BC, Canada). A 40×, 0.8 numerical aperture (NA) fluorite water-immersion objective (Nikon) was used. Whole-cell recordings were performed using borosilicate glass capillaries pulled on a P-97 puller (Sutter Instrument, Novato, CA), and filled with EGTA-free, high-K^+ intracellular solution designed to mimic the intracellular electrolyte concentration composed of (in μM) K-gluconate, 124; HEPES, 40; Mg-ATP, 4; guanosine 5′-triphosphate, 0.4 mM; phosphocreatine, 10; and $MgCl_2$, 2. The internal solution was supplemented with the Ca^{2+}-sensitive probes described below. Control (CTRL) cells were recorded with the intracellular solution containing 0.2 mM EGTA and without calcium probes. Osmolarity was adjusted to approximately 270–290 mOsm and pH to 7.3. The pipette resistance was 3–5 MΩ. All recordings were made using a Multiclamp 700B amplifier (Molecular Devices, Sunnyvale, CA) in current clamp mode. Both series resistance and liquid junction potential were compensated for. The average series resistance in voltage clamp configuration was 8.0 ± 0.3 MΩ prior to >60% compensation (>14 KHz correction bandwidth; equivalent to <10 msec lag). Average bridge values in current clamp configuration were 17.4 ± 0.4 MΩ. Analog signals were low-pass filtered at 2 kHz, and digitized at 10 kHz using the Digidata-1440A interface and pClamp10 software (Molecular Devices). A holding current of ≤80 pA was used to maintain resting membrane potential of −50 mV if necessary.

The recording region was located mainly in the pars compacta in the posterior PPN, immediately dorsal to the superior cerebellar peduncle. This area of the PPN has been shown to have the highest cell density (44, 45). Gigaseal and further access to the intracellular neuronal compartment were achieved in voltage clamp mode, with the holding potential set at −50 mV (i.e., near the resting membrane potential of PPN neurons). Soon after the membrane was ruptured, the intracellular solution and dyes were allowed to equilibrate for 10 min without significant changes in either series resistance (bridge compensation in current clamp mode) or membrane capacitance values before imaging recordings were performed. Experiments lasted 15 to 25 min from breaking into the cell to experiment completion. Calcium-mediated activity was studied in current clamp mode in the presence of synaptic blockers (SB, see above) and tetrodotoxin (TTX, 3 μM) to block sodium channels and action potential generation. The membrane potential was depolarized in a ramp-like fashion from −50 mV [a membrane potential known to inactivate T-type calcium channels (20, 21)] over a period of 2 sec until oscillations were elicited (20, 21). At the peak of the ramp, 200–500 pA was injected.

Drug application. Bath-applied drugs were administered to the slice via a peristaltic pump (Cole-Parmer, Vernon Hills, IL) and a three-way valve system such that solutions reached the slice 1 min after the start of application. The sodium channel blocker TTX (3 μM) was purchased from Sigma (St. Louis, MO). Channel blockers were purchased from either Peptide International (Louisville, KY) or Alomone Labs (Jerusalem, Israel). We used cadmium chloride (Cd^{+2}, 100 μM), a nonspecific, voltage-dependent calcium channel blocker; ω-agatoxin-IVA (AgA; 100–200 nM), a specific P/Q-type calcium channel blocker; and ω-conotoxin-GVIA (CgTx; 1.5–2.5 μM), a specific N-type calcium channel blocker. Blockers were bath-applied for ≥10 min before testing.

Ca^{2+} indicators. Calcium imaging in the PPN has never been reported. Previous work on the Pf described comparative studies of a number of fluorescent probes to determine optimal quantum yield, photo bleaching and quenching, in addition to cell permeability, lifetime in a living cell, and toxicity (14). Our previous calcium imaging studies in the Pf showed that ratiometric calcium probes were unable to adequately visualize calcium oscillations due to acquisition speed limitations; however, single-wavelength indicators such as Oregon Green BAPTA 1 (OGB1) were capable of showing oscillations (14). To allow high-speed ratiometric image acquisition, we developed a novel method using OGB1 compared with a coinjected calcium-insensitive fluorescent dye, Chromeo 494 (CHR; Active Motif; Carlsbad, CA). This novel method was used in combination with Fura 2 and Bis Fura to provide an assessment of calcium levels, because these are the standard calcium indicators used in the field, and served as standards to compare with the OGB1/CHR indicator.

CHR is a long-stokes-shift dye, excited at 494 nm and emitting at 628 nm. This allows simultaneous excitation with OGB1 (absorbs at 488 nm; emits at 520 nm), and the emitted light from each dye can be separated with the appropriate optics. Fura 2, Bis Fura, and OGB1 were purchased from Invitrogen (Grand Island, NY). Fura 2 (200 μM), Bis Fura (200 μM), OGB1 (100 μM), and CHR (50 μM) were loaded with the intracellular solution. Some cells were coinjected with Alexa-594 Hydrazide (Invitrogen, 50 μM) as a volumetric marker. Early calcium imaging experiments used 200 μM OGB1, but pilot studies using light-emitting diode (LED) illumination revealed lower concentrations of OGB1 were optimal (see RESULTS).

Ca^{2+} imaging. Cells were illuminated with a Lambda DG-4 high-speed wavelength switcher equipped with a 300-W xenon arc bulb (Sutter Instruments) for Fura 2 and Bis Fura experiments. Single-

wavelength OGB1 and OGB1/CHR experiments were illuminated with a custom-built, high-power LED lamp. The lamp consisted of a 4.1-V, 18-A blue LED (CBT-120-B-C11-KJ300; Luminus Devices, Billerica, MS) with 462 nm peak output. The LED was powered by a simple circuit consisting of a rechargeable, sealed lead acid battery, and a high-power 1-Ω current-limiting resistor. The LED was passively cooled with a large heat sink and directly coupled to the microscope by an antireflection-coated aspheric lens (350–700 nm; 40 mm focal length; Thorlabs, Newton, NJ). Indicator-filled neurons were visualized at 64 × 64 pixels with an Evolve 128 EMCCD camera (Photometrics, Tucson, AZ) operating with a 2× bin with a low EM gain (typically ~20×) for high-speed experiments. Fura 2 and Bis Fura exposures were acquired in pairs with exposures of 2.5 msec (400 frames/s) with ~1.2 msec wavelength switching time. Fura 2 and Bis Fura specimens were illuminated with alternating 380- and 340-nm excitation light and recorded using a 510/80× emission filter. Fura 2 and Bis Fura fluorescence changes are represented as the ratio 340/380 throughout. When the area under the curve was integrated, the units are expressed as (340/380)*msec, in which the symbol * represents multiplication, because use of the symbol × could be mistaken for a constant.

OGB1/CHR image streams were acquired with synchronized dual Evolve 128 cameras operating with a 2× bin with a low EM gain using 2-msec exposures (500 frames/s). Quant-view mode was used on both cameras. The optical pathway used a filter cube equipped with a 480/40× excitation filter and 510-nm beam splitter. The emission light was directed to a DC2 two-channel, full-field dual-cam system (Photometrics, Tucson, AZ). The dual cam uses a filter/mirror system to split the emitted light into two separate spatially identical, full-field light pathways. A 565-nm beam splitter was used split the light with a 520/30× or a 630/50× emission filter used on each light path. On the other hand, single-wavelength OGB1 wide-field experiments were acquired with the Evolve 512 operating in quant view with a 1× bin with a low EM gain using 40-msec exposures (25 frames/s). A 480/40× excitation filter was used with a 510-nm beam splitter and 535/50× emission filter.

All image streams were saved continuously in computer RAM using Metamorph software (Molecular Devices, Sunnyvale, CA), and subsequently saved to the hard disk. All imaging and recording synchronization was accomplished through pCLAMP Clampex software. All images were processed in ImageJ (30) where they were background-corrected using the European Molecular Biology Laboratory tools plug-in with the simple ratio correction method (26), applied a three-dimensional median filter (15), and registered with the Registax plug-in (42). Ratio images were processed with the Ratio Plus plug-in. Delta F/F images were generated for single wavelength OGB1 experiments. Image stacks were analyzed in Metamorph. Pixel regions (3 × 3) of interest were extracted from each image. Extracted fluorescence recordings were analyzed in OriginPro (OriginLab, Northampton, MA).

Calcium calibration was accomplished with a calibration buffer kit from Invitrogen (C-3008MP) using protocols outlined by Invitrogen and previously used in our laboratory (14). The kit contains two buffers with 30 mM MOPS at pH 7.2 in 100 mM KCl, one buffer with 39 μM free Ca^{2+} and the other with zero free Ca^{2+}. This kit does not perfectly match the intracellular conditions present, but it does mimic the osmotic pressure and pH of the intracellular solution used and allows us to confirm the K_d in our system. The kit employs a reciprocal dilution method to minimize indicator concentration errors (19, 40). Each buffer solution was visualized in our imaging system and fluorescence intensities were recorded.

Confocal imaging. Upon completing Ca^{2+} imaging, the patch electrode was carefully removed to maintain cell structure. Slices were fixed overnight in 4% paraformaldehyde at 4°C. The slices were then washed with 0.1 M phosphate buffer and mounted with Fluoromount (Sigma). Slices were examined with a Nikon AZ100 multizoom fluorescence microscope to determine suitability for confocal scanning. Intact neurons were scanned on a Zeiss PASCAL LSM 5 confocal microscope (Oberkochen, Germany) with a 40× 0.8 NA objective. Alexa 594 was illuminated with 543-nm excitation light. Image stacks were acquired at 1024 × 1024 with 4× averaging. Stacks were deconvoluted and processed with Amira software (Visualization Sciences Group, Burlington, MA).

Histology. Several slices with cells containing Alexa Fluor 594 were processed for brain nitric oxide synthase (bNOS) immunofluorescence (selective label for cholinergic PPN cells). Slices were lightly fixed in fresh 4% paraformaldehyde for 1 h at 4°C then rinsed 2 × 5 min in 0.01 M phosphate buffer (PB). Slices were then incubated for 72 h in chicken anti-bNOS monoclonal antibody (1:400 dilution) at 4°C. Slices were washed 3 × 25 min in 0.01 M PB and labeled with Alexa Fluor 488 goat anti-chicken secondary antibody for 2 h. The slices were washed 4 × 5 min then mounted using Sigma Fluoromount and Invitrogen secure-seal spacers. Cells were visualized on a Zeiss Axioskop 2 at 20× with a QICAM camera. Standard red and green fluorescence filter cubes were used.

Data analysis. Off-line analyses were performed using Clampfit software (Molecular Devices). Comparisons between groups were carried out using Student's *t*-test with Bonferroni correction, and ANOVA with Bonferroni post hoc testing using OriginPro. Power spectra were compiled from current clamp recordings using ramps. All data were tested for normality using the D'Agostino-Pearson omnibus test and were normally distributed ($P \geq 0.05$). Fluorescence curve areas were calculated for the full record using the integration function in OriginPro. Differences were considered significant at $P \leq 0.05$. All results are presented as means ± SE.

RESULTS

Whole-cell patch-clamp recordings were performed on a total of 121 PPN neurons. Calcium transients were recorded in 67 cells without EGTA, whereas 54 were recorded without calcium probes using an EGTA intracellular solution. All cells were localized and identified by cell type as previously described (9, 10, 35). Cells were localized to the region immediately dorsal to the superior cerebellar peduncle (Fig. 1*A*). The cell morphology was as previously described with both multipolar and fusiform neuronal shapes with high variation in number of primary dendrites (approximately 2–6 primary dendrites) (31). Figure 1*B* is an example of a cell filled with Alexa Fluor 594 while being studied, showing the fusiform multipolar nature of the cell in situ. Figure 1*C* is an example of a confocal reconstruction of a filled (Alexa Fluor 594) PPN neuron in fixed tissue. Figure 1*D* provides a wide-field view of the PPN in tissue processed for bNOS immunocytochemistry showing cholinergic cells as green fluorescence, and the recorded cell (Alexa Fluor 594 labeled orange) also labeled with bNOS (yellow merged view).

Hyperpolarizing current pulses were applied in current clamp mode to determine the presence of LTS or Ia-mediated membrane potential deflections to determine cell type (8, 9, 35). All cell types in the PPN manifest gamma oscillations (21, 35), and thus were pooled in this study. No differences in average resting membrane potential were observed in dye-filled PPN neurons across cell type (type I, −50 ± 2 mV, n = 12; type II, −52 ± 1 mV, n = 27; type III, −54 ± 1 mV, n = 28; one-way ANOVA, $F_{2,64} = 1.98$, $P = 0.15$, $n = 67$). However, if the resting membrane potential was segregated by calcium indicator type, significant differences were found between OGB1/CHR and the two Fura-based indicators. Significant differences were also observed between the two Fura-based indicators and control cells, whereas no significant differences were

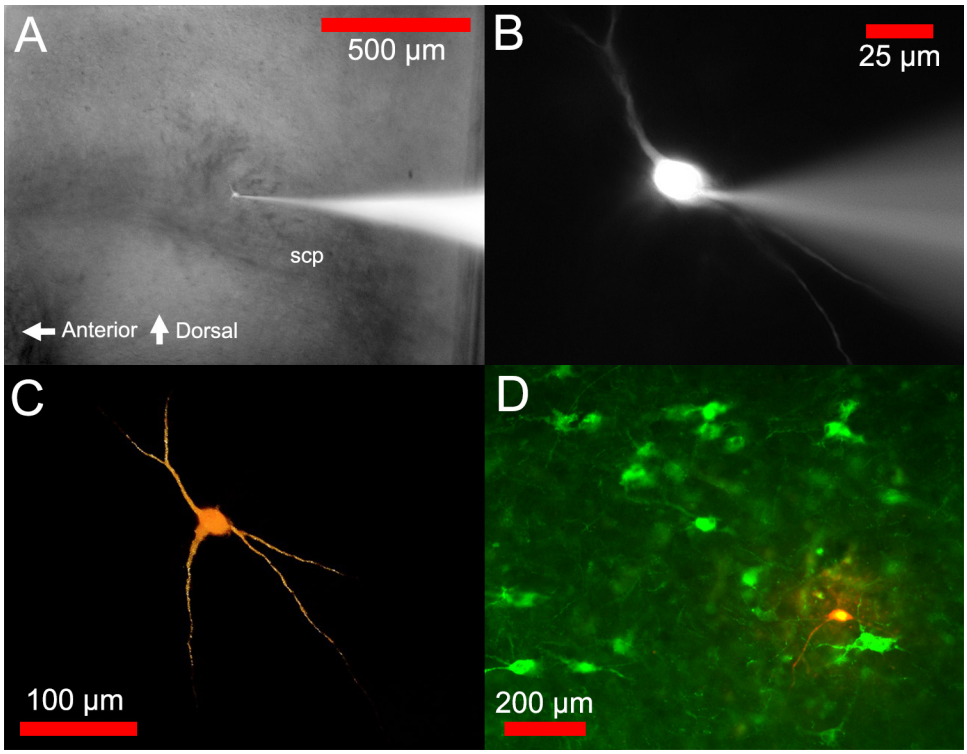

Fig. 1. Localization and morphology of PPN neurons. *A*: the PPN is a wedge-shaped cellular region overlapping the superior cerebellar peduncle (SCP). Hybrid brightfield and fluorescence image showing the location of a single recorded neuron in the PPN pars compacta dorsal to the SCP. *B*: wide-field fluorescence image of the same neuron identified with intracellular injection of Alexa Fluor 594. Note the multipolar shape with multiple primary dendrites. *C*: maximum projection confocal image of the same Alexa Fluor 594-filled neuron. *D*: wide-field image of a different Alexa Fluor-filled neuron with brain nitric oxide synthase immunofluorescence labeling (*green*) of cholinergic PPN neurons. Note the *red/green* (*yellow* nucleus) colocalization indicating that the recorded neuron was a cholinergic cell.

found between OGB1/CHR and control cells (Fura 2, −49 ± 1 mV; Bis Fura, −51 ± 2 mV; OGB1/CHR, −56 ± 1 mV; CTRL, −55 ± 1 mV; one way ANOVA, $F_{3,107} = 8.87$, $P = 2.7 \times 10^{-5}$, $n = 111$; post hoc testing, Fura 2 vs. CTRL, $P = 5.15 \times 10^{-4}$; Bis Fura vs. CTRL, $P = 0.04$; OGB1/CHR vs. CTRL, $P = 1.0$; Fura 2 vs. Bis Fura, $P = 1.0$; OGB1/CHR vs. Fura 2, $P = 2.5 \times 10^{-4}$; OGB1/CHR vs. Bis Fura, $P = 0.02$).

Differences in resting membrane potential mediated by OGB1/CHR were not due to changes in total input resistance (average slopes from V-I curves were CTRL 290 ± 32 MΩ, $n = 9$; OGB1/CHR 291 ± 56 MΩ, $n = 9$; $P = 0.99$). The V-I curve R^2 values were >0.95.

Calibration. The calcium affinity for each indicator was calculated as previously described (14). A series of known concentration calcium buffers were visualized and a K_d value for each indicator was calculated. The calibration curves were calculated from averages of four calibration experiments preformed on each dye. As expected, OGB1/CHR showed the highest affinity with a $K_d = 109 \pm 16$ nM. This was followed by Fura 2 with a $K_d = 334 \pm 8$ nM, and Bis Fura had the lowest affinity with a $K_d = 953 \pm 3$ nM.

Calcium concentration measurements. Ratiometric measurements converted to calcium concentrations demonstrated resting concentrations of 62 ± 16 nM at somatic levels ($n = 12$) and 149 ± 27 nM at dendritic levels ($n = 12$) for Fura 2. For Bis Fura, levels of 73 ± 6 nM at somatic ($n = 12$) and 158 ± 15 nM at dendritic ($n = 10$) compartments were observed. OGB1/CHR showed a resting somatic concentration of 56 ± 12 nM somatic ($n = 13$) and 114 ± 18 nM dendritic ($n = 11$) concentrations. The calcium transients during the current ramp showed a peak of 130 ± 26 nM at somatic ($n = 12$) and 256 ± 27 nM at dendritic ($n = 12$) levels for Fura 2; and 158 ± 7 nM at somatic ($n = 12$) and 334 ± 19 nM at dendritic ($n = 10$) compartments for Bis Fura. The peak OGB1/CHR somatic concentration was 107 ± 17 nM ($n = 13$), with a peak dendritic concentration of 180 ± 16 nM ($n = 11$). The percent change of the calcium concentration between the level at baseline and the level at the peak of the applied ramp was calculated for somatic and dendritic compartments (somatic: Fura 2, 205 ± 76%; Bis Fura, 128 ± 15%; OGB1/CHR, 172 ± 64%; dendritic: Fura 2, 120 ± 36%; Bis Fura, 123 ± 15%; OGB1/CHR, 92 ± 27%).

Statistical testing of both somatic and dendritic calcium concentrations revealed significant differences between baseline (before the ramp) and peak (at the peak of the ramp) calcium concentrations for each indicator (somatic: Fura 2 $P = 0.03$, Bis Fura $P = 8.7 \times 10^{-9}$, OGB1/CHR $P = 0.02$; dendritic: Fura 2 $P = 0.009$, Bis Fura $P = 9.1 \times 10^{-7}$, OGB1/CHR $P = 0.01$). These results suggest that all indicators showed a significant increase at the peak of the ramp. However, statistical comparison of baseline values from the soma vs. the dendrites showed no significant differences (ANOVA, $F_{2,32} = 0.46$, $P = 0.6$). This suggests that there were significant increases at both somatic and dendritic compartments after the ramp. Percent change for each somatic and dendritic indicator group showed no significant differences between indicators (somatic percent change ANOVA, $F_{2,32} = 0.46$, $P = 0.6$; dendritic percent change ANOVA, $F_{2,20} = 0.34$, $P = 0.7$). Thus, each indicator can be considered interchangeable for measuring ramp-evoked calcium transients in PPN neurons.

Depolarizing ramps generated calcium transients throughout PPN neuronal intracellular compartments. We tested the hypothesis that in the presence of TTX (to prevent action potential generation and synaptic activity) and synaptic blockers (to prevent activation by spontaneous release of common inputs), depolarizing current ramps will induce measureable

calcium transients throughout PPN neurons. Figure 2 shows representative cells recorded using each indicator [from left to right: the electrical record (Fig. 2*A*), the power spectrum of the electrical record (Fig. 2*B*), the fluorescence signal (Fig. 2*C*), a graph of the area under the curve of the fluorescence signal at the some (Fig. 2*D*), and at the proximal dendrites (Fig. 2*E*)]. Each neuron was depolarized using a current ramp in current-clamp mode, which induced calcium-channel-mediated oscillations regardless of dye (Fig. 2*A*, *black records*). The recorded frequencies ranged from alpha (8–13 Hz) to beta/low gamma (20–40 Hz) (Fig. 2*B*, *black lines*). Although the oscillation frequency appears to be low in some of the cells shown, the average frequency for all cells was in the alpha/beta range (19 ± 5, n = 40), which is slightly lower than previously described for cells recorded without calcium indicators (21). Fluorescence recordings showed an increase in signal coin-

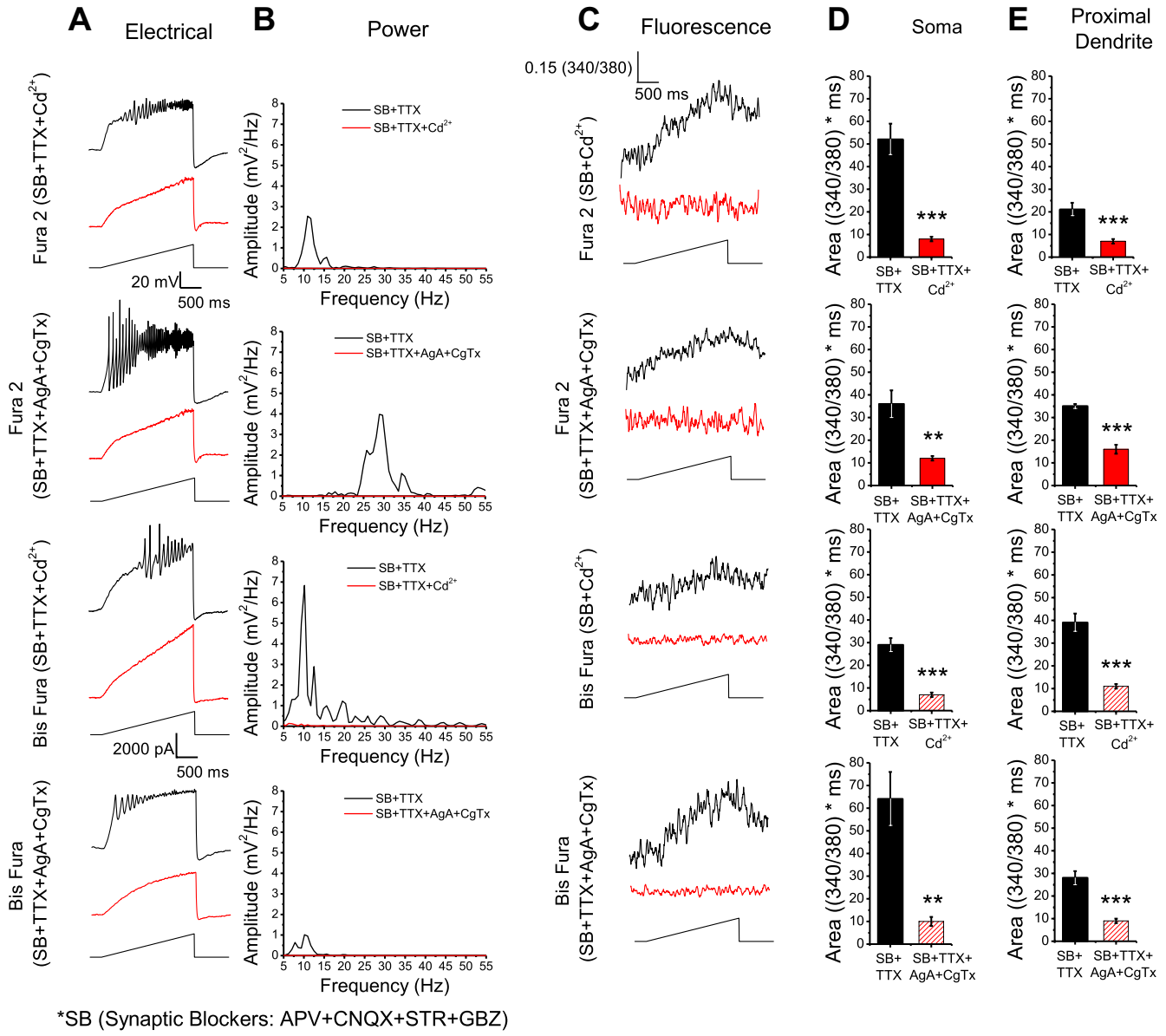

Fig. 2. Depolarizing current ramps generated oscillations and measureable intracellular calcium transients. *A*: representative oscillations of a PPN neuron (*black records*), and in the presence of the nonspecific calcium channel blocker Cd^{2+} (*red records* in *top* and *third rows*) or specific calcium channel blockers AgA and CgTx (*red records* in *second* and *fourth rows*) recorded during 2-sec-long ramps. Note that calcium oscillations were eliminated by Cd^{2+}, AgA, and CgTx, indicating fluorescence (*C*) was mediated by N-type and P/Q-type calcium channels. *B*: overlapping recordings comparing power spectrum amplitudes for oscillations present in *A*, before and after channel blockers. *C*: somatic fluorescent transients induced by the current ramp (*black record*) recorded simultaneously with the oscillations present in *A*. Note how both membrane oscillations and intracellular calcium fluorescence signals were eliminated after blockers were applied (*red record*). *D*: bar graph showing the average integrated somatic curve area for the fluorescence curves before Cd^{2+} [*black bar*: Fura 2, 51 ± 7 (340/380)*msec, n = 12; Bis Fura, 29 ± 3 (340/380)*msec, n = 12] and after Cd^{2+} [*red bar*: Fura 2, 8 ± 1 (340/380)*msec; Bis Fura, 7 ± 1 (340/380)*msec]. Fluorescence curves before AgA and CgTx [*black bar*: Fura 2, 36 ± 6 (340/380)*msec, n = 8; Bis Fura, 64 ± 12 (340/380)*msec, n = 8] and after AgA and CgTx [*red bar*: Fura 2, 12 ± 1 (340/380)*msec; Bis Fura, 10 ± 2 (340/380)*msec]. *E*: bar graph showing the average integrated proximal dendritic curve area before Cd^{2+} [*black bar*: Fura 2, 21 ± 3 (340/380)*msec, n = 14; Bis Fura, 39 ± 4 (340/380)*msec, n = 10] and after Cd^{2+} [*red bar*: Fura 2, 7 ± 1 (340/380)*msec; Bis Fura 2, 11 ± 1 (340/380)*msec]. Fluorescence curves before AgA and CgTx [*black bar*: Fura 2, 35 ± 1 (340/380)*msec, n = 5; Bis Fura, 28 ± 3 (340/380)*msec, n = 16] and after AgA and CgTx [*red bar*: Fura 2, 16 ± 2 (340/380)*msec; Bis Fura, 9 ± 1 (340/380)*msec].

ciding with the increase in current during the ramps (Fig. 2*C*, *black records*). We then used the nonspecific calcium-channel blocker cadmium (Cd^{2+}) to determine whether the electrical and fluorescence signals were due to calcium flux (Fig. 2 *top* and *third rows, left* to *right*). The *top row* shows that using Fura 2, the addition of Cd^{2+} blocked the ramp-induced oscillations (Fig. 2*A*, *red record*), eliminating activity in the power spectrum of the electrical record (Fig. 2*B*, *red line*). The simultaneously acquired fluorescence signal was also blocked by Cd^{2+} (Fig. 2*C*, *red record*). In the presence of Cd^{2+}, both the somatic (Fig. 2*D*) and dendritic (Fig. 2*E*) areas under the curve of the fluorescence signal decreased significantly. Similar results were observed using Bis Fura (Fig. 2, *third row*).

We then used the specific P/Q-type channel blocker AgA in combination with the specific N-type calcium channel blocker CgTx to determine whether the electrical and fluorescence signals were due to calcium flux through N- and P/Q-type calcium channels (Fig. 2, *second* and *fourth rows left* to *right*). The *second row* shows that using Fura 2, the addition of AgA+CgTx blocked the ramp-induced oscillations (Fig. 2*A*, *red record*), eliminating activity in the power spectrum of the electrical record (Fig. 2*B*, *red line*). The simultaneously acquired fluorescence signal was also blocked by AgA+CgTx (Fig. 2*C*, *red record*). In the presence of AgA+CgTx, both the somatic (Fig. 2*D*) and dendritic (Fig. 2*E*) areas under the curve of the fluorescence signal decreased significantly. Similar results were observed using Bis Fura (Fig. 2, *fourth row*).

Figure 3 provides the same results for OGB1/CHR. The presence of calcium transients in OGB1/CHR recordings demonstrates that regardless of the high affinity for calcium of this dye, the combination of both dyes is viable for measuring

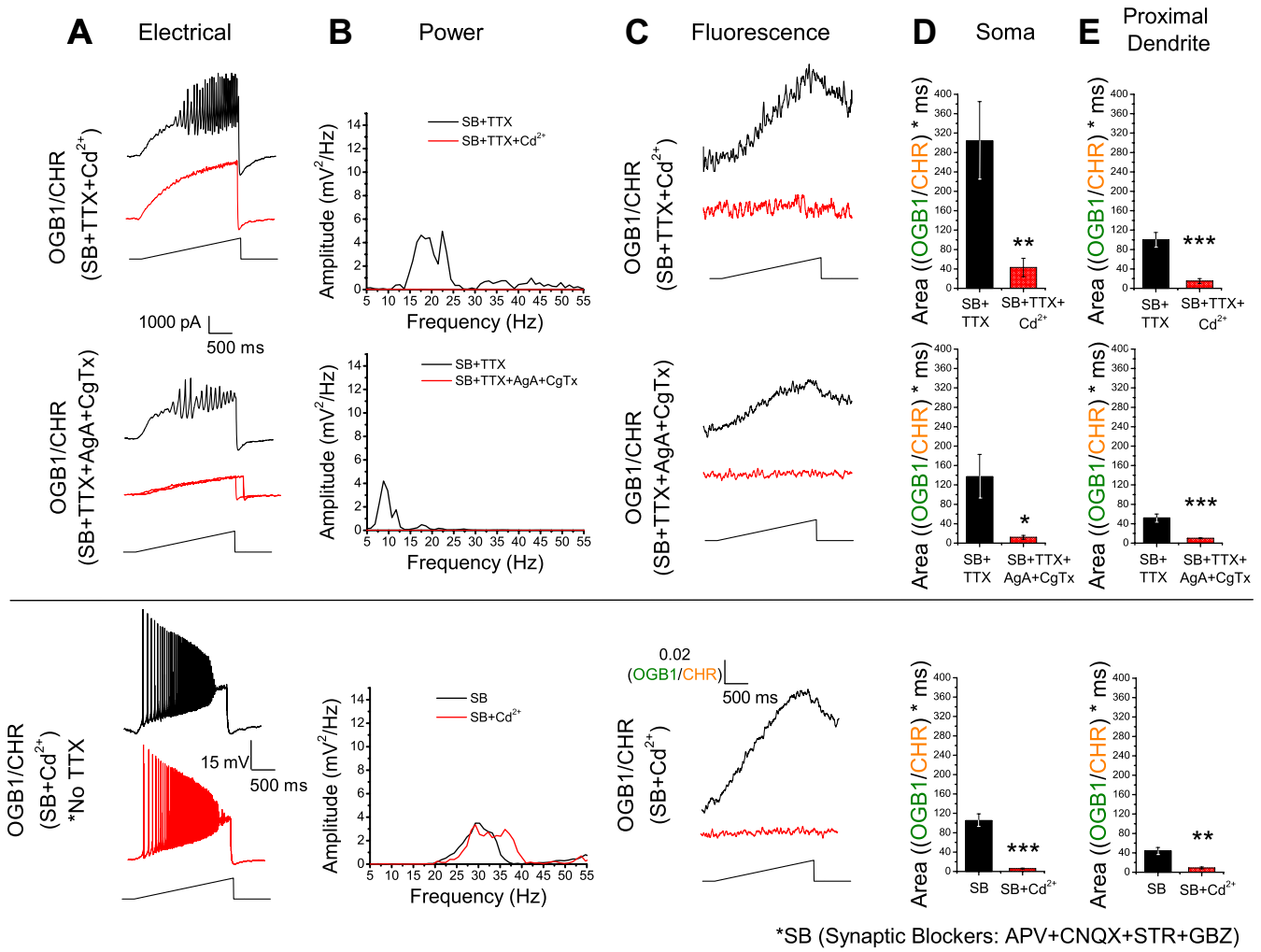

Fig. 3. N-type and P/Q-type calcium channel-mediated calcium oscillations in the PPN visualized with OGB1/CHR. The two rows above the horizontal line used both synaptic blockers (SB) and TTX; however, the lower row used only synaptic blockers. *A*: patch-clamp recorded calcium oscillations before (*black record*) and after (*red record*) specific and nonspecific calcium channel blockers. *B*: power spectra of records in *A*. *C*: fluorescence recordings acquired simultaneously with electrical recordings in *A*, with (*red record*) and without (*black record*) calcium channel blockers. *D*: bar graph showing the average integrated area under the curve for the fluorescence recordings before Cd^{2+} [*black bar*: SB only 105 ± 14 (OGB1/CHR)*msec, $n = 7$; with TTX 301 ± 81 (OGB1/CHR)*msec, $n = 10$] and after Cd^{2+} [*red bar*: SB only 5 ± 2 (OGB1/CHR)*msec; with TTX 43 ± 19 (OGB1/CHR)*msec]. Before AgA and CgTx [*black bar*: 137 ± 46 (OGB1/CHR)*msec, $n = 10$] and after [*red bar*: 12 ± 4 (OGB1/CHR)*msec]. *E*: bar graph showing the average integrated area under the curve for proximal dendritic fluorescence before Cd^{2+} [*black bar*: SB only 44 ± 7 (OGB1/CHR)*msec, $n = 8$; with TTX 100 ± 15 (OGB1/CHR)*msec, $n = 21$] and after Cd^{2+} [*red bar*: SB only 9 ± 2 (OGB1/CHR)*msec; with TTX 15 ± 5 (OGB1/CHR)*msec]. Before AgA and CgTx [*black bar*: 52 ± 8 (OGB1/CHR)*msec, $n = 17$] and after [*red bar*: 10 ± 1 (OGB1/CHR)*msec]. *$P < 0.05$; **$P < 0.01$; ***$P < 0.001$.

intracellular calcium concentrations. We first analyzed the electrical responses and fluorescence calcium transients using synaptic blockers only, and omitting TTX (Fig. 3, *top row*). We tested whether the area under the fluorescence curve changed when TTX was omitted to determine whether this caused calcium channels to be inactivated by unclamped nearby synaptic neuronal activity as well as by recurrent overactivation of PPN dendritic compartments. We used only OGB1/CHR rather than all of the other calcium indicators for this series of experiments. The electrical record shows action potentials occurring both before and after the addition of Cd^{2+} (Fig. 3*A*, *black* before Cd^{2+}, *red* after Cd^{2+}). The power spectra show that the action potentials were approximately at the same frequencies before and after the addition of Cd^{2+} (Fig. 3*B*, *red* and *black lines*). However, the fluorescence signal that was present when SB were used (Fig. 3*C*, *black record*) was eliminated when Cd^{2+} was used (Fig. 3*C*, *red record*). This result shows that the absence of TTX allowed the electrical manifestation of action potentials during the ramp (Fig. 3*A*), but the fluorescence signal (Fig. 3*C*), because it was entirely due to calcium, was blocked by Cd^{2+}. This further confirms that the fluorescence signal was generated only by calcium flux and was unchanged by the absence of TTX. Moreover, the average areas under the fluorescence curve for OGB1/CHR for both the soma [105 ± 14 (OGB1/CHR)*msec, $n = 7$] and proximal dendrite [44 ± 7 (OGB1/CHR)*msec, $n = 8$] showed a significant decrease in fluorescence when Cd^{2+} was bath-applied for both soma [5 ± 2 (OGB1/CHR)*msec, $P = 3.8 \times 10^{-4}$] and proximal dendrite areas [9 ± 2 (OGB1/CHR)*msec, $P = 0.001$] (Fig. 3, *D* and *E*, *top*) without TTX (bottom row, *D* and *E*).

We then carried out recordings using OGB1/CHR in the presence of SB+TTX (Fig. 3 *second* and *third rows*). The *second row* shows that Cd^{2+} blocked the ramp-induced oscillations in the electrical recording (Fig. 3, *A* and *B*, compare *black* vs. *red record* and *line*). Similarly, Cd^{2+} blocked the fluorescence recording (Fig. 3*C*) and reduced the area under the fluorescence curve in the soma (Fig. 3*D*) and dendrite (Fig. 3*E*). These results showed that the oscillations and the fluorescence signals using OGB1/CHR were due to calcium flux (Fig. 3), similarly to the other indicators (Fig. 2). In addition, we used the specific N- and P/Q-type calcium-channel blockers AgA+CgTx to eliminate the oscillations in the electrical record (Fig. 3*A*, *third row*), as well as the fluorescence signal (Fg. 3*C*), soma area under the curve (Fig. 3*D*), and dendrite under the curve (Fig. 3*E*). This confirmed that that fluorescence signal using OGB1/CHR was indeed mediated by N- and P/Q-type calcium channels. We should also note that the somatic fluorescence records did not show a difference between cells recorded with (Fig. 3, *top row*) and without (Fig. 3, *bottom row*) TTX ($P = 0.06$). In addition, although the calcium fluorescence recordings did not appear to show a difference (Fig. 3*C*, compare *top* and *second rows*), surprisingly, the calcium transient areas appeared to increase when comparing recordings with and without TTX (Fig. 3, *D* and *E*, compare *top row* vs. *second row*).

Integrated areas. The average integrated area under the curve of the fluorescence transients recorded in both the soma [Fura 2, 51 ± 7 (ratio 340/380)*msec, $n = 12$; Bis Fura, 29 ± 3 (ratio 340/380)*msec, $n = 12$; OGB1/CHR, 301 ± 81 (OGB1/CHR)*msec, $n = 10$] and proximal dendrite [Fura 2, 21 ± 3 (ratio 340/380)*msec, $n = 14$; Bis Fura, 39 ± 4 (ratio 340/380)*msec, $n = 10$; OGB1/CHR, 100 ± 15 (OGB1/CHR)*msec, $n = 21$] decreased significantly for both the soma recordings [Fura 2, 8 ± 1 (ratio 340/380)*msec, $P = 1.2 \times 10^{-4}$; Bis Fura, 7 ± 1 (ratio 340/380)*msec, $P = 4 \times 10^{-6}$; OGB1/CHR, 43 ± 19 (OGB1/CHR)*msec, $P = 0.004$] and dendrite recordings [Fura 2, 7 ± 1 (ratio 340/380)*msec, $P = 7.4 \times 10^{-5}$; Bis Fura, 11 ± 1 (ratio 340/380)*msec, $P = 8 \times 10^{-5}$; OGB1/CHR, 15 ± 5 (OGB1/CHR)*msec, $P = 3.9 \times 10^{-6}$] using a Student's *t*-test (Fig. 2, *D* and *E*; Fig. 3, *D* and *E*). Furthermore, the area of fluorescence transients from the soma was significantly larger than in the dendrites using Fura 2 and OGB1/CHR (Fura 2 $P = 0.001$; Bis Fura $P = 0.2$; OGB1/CHR $P = 0.001$). Note that OGB1/CHR had a higher area fluorescence level that can be attributed to the OGB1/CHR indicator being brighter and more sensitive than either of the Fura derivatives. However, statistical testing showed no significant difference between the somatic precadmium transient areas ($P = 0.19$) or dendritic transient areas ($P = 0.16$).

Our previous work showed that calcium oscillations in the Pf are due to P/Q- and N-type voltage-dependent calcium channels (20). We studied the effects of both AgA (a specific P/Q-type calcium-channel blocker) and CgTx (a specific N-type calcium-channel blocker), to confirm that P/Q- and N-type calcium channels were responsible for the observed fluorescent calcium transients in the PPN ($n = 26$). As described above, the combination of AgA and CgTx abolished electrical oscillations (*red records* in Fig. 2, *A* and *B*; Fig. 3, *A* and *B*), as well as calcium transients (*red records* in Fig. 2*C* and Fig. 3*C*). The average integrated area under the curve for fluorescence at the soma [Fura 2, 36 ± 6 (ratio 340/380)*msec, $n = 8$; Bis Fura, 64 ± 12 (ratio 340/380)*msec, $n = 8$; OGB1/CHR, 137 ± 46 (OGB1/CHR)*msec, $n = 10$] and dendrite [Fura 2, 35 ± 1 (ratio 340/380)*msec, $n = 5$; Bis Fura, 28 ± 3 (ratio 340/380)*msec, $n = 16$; OGB1/CHR, 52 ± 8 (OGB1/CHR)*msec, $n = 17$] showed a significant decrease in both the soma [Fura 2, 12 ± 1 (ratio 340/380)*msec, $P = 0.002$; Bis Fura, 10 ± 2 (ratio 340/380)*msec, $P = 0.002$; OGB1/CHR, 12 ± 4 (OGB1/CHR)*msec, $P = 0.02$] and dendrite [Fura 2, 16 ± 2 (ratio 340/380)*msec, $P = 2.4 \times 10^{-5}$; Bis Fura, 9 ± 1 (ratio 340/380)*msec, $P = 6.5 \times 10^{-7}$; OGB1/CHR, 10 ± 1 (OGB1/CHR)*msec, $P = 7.6 \times 10^{-5}$] across dyes (Figs. 2 and 3).

PPN cell types are partly segregated in terms of neurotransmitter, with type I cells being noncholinergic, type II cells being two-thirds cholinergic, and type III cells being one-third cholinergic (8, 9, 35). Interestingly, when all of the Cd^{2+} and AgA/CgTx somatic data were pooled, we observed no significant difference in percent area across the three electrophysiological cell types (type I 83 ± 3%, $n = 11$; type II 78 ± 3%, $n = 24$; type III 79 ± 4%, $n = 25$; ANOVA, $F_{2,57} = 0.3$, $P = 0.74$). However, if the Cd^{2+} and AgA/CgTx dendritic data were pooled, we observed that type II cells had a significantly lower percent area than types I and III, whereas there was no significant difference between type I and type III cells (type I 76 ± 3%, $n = 14$; type II 63 ± 3%, $n = 27$; type III 74 ± 2%, $n = 37$; ANOVA, $F_{2,75} = 6.5$, $P = 0.002$; post hoc test type I vs. type II $P = 0.01$; type I vs. type III $P = 0.87$; type II vs. type III $P = 0.006$). These results suggest that in general, cholinergic PPN neurons, which are mainly type II, may manifest lower calcium signals than noncholinergic neurons. This is in agreement with our results showing that type II cells

manifest lower amplitude ramp-induced calcium oscillations compared with type I and type III PPN cells (21).

Calcium oscillations were evident in the calcium-dependent fluorescence signal. Previous experiments in the Pf attempted to use ratiometric indicators such as Fura 2 or Indo to simultaneously record calcium oscillations in both the electrical and fluorescence recordings (14). These revealed that normal ratiometric calcium indicators were poor tools for studying high-speed calcium oscillations. Thus we originally resorted to using OGB1, a single-wavelength calcium indicator, which could be imaged at higher acquisition speeds. However, OGB1 is still susceptible to multiple imaging issues related to dye variation from cell to cell. To use OGB1 for ratiometric analysis, Chromeo 494 (noncalcium-sensitive) was coinjected to provide baseline fluorescence measurements. The OGB1/CHR ratio indicator was used to record calcium transients at high frame rates to test the hypothesis that individual calcium oscillations observed in the electrical recordings were also present in the fluorescence calcium recordings. Simultaneous electrical and fluorescence oscillations were observed in 14 OGB1/CHR-filled neurons, with a representative neuron shown in Fig. 4 (all panels). The combination of LED illumination along with the OGB1/CHR indicator allowed fluorescence recordings to demonstrate individual calcium oscilla-

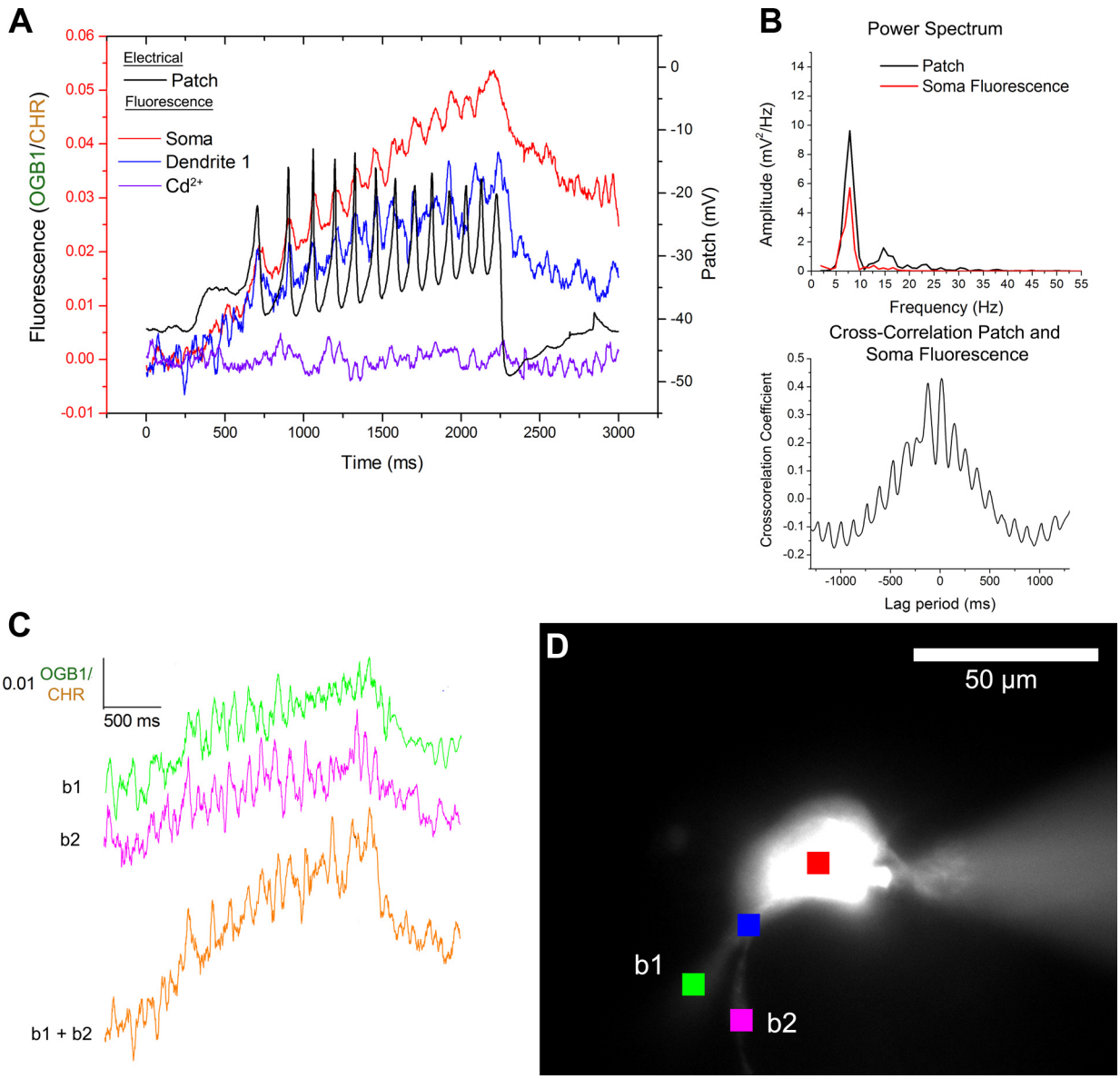

Fig. 4. Oscillations present in the electrical signal were also evident in the recorded dendritic calcium signal. *A*: records of elicited calcium oscillations recorded simultaneously with both electrical recording (*black record*) and high-speed fluorescence imaging (*red, blue,* and *purple records*). The oscillations in the somatic fluorescence recording (*red record*) closely matched those in the electrical record. The *blue dendritic record* also followed the electrical record, but with more variation. Note that fluorescence was mostly eliminated by the addition of Cd^{2+} in the *purple record*. *B*: power spectrum and cross-correlation graph of the electrical record (*black record*) and the somatic fluorescence record (*red record*). *C*: two dendritic branches (*b1 green, b2 pink*) originating from the proximal dendrite in *A* (*blue record*). Both branches were summed (*b1+b2 orange record*) to yield a signal closely matching the oscillations in the proximal dendrite (*blue* in *A* and *D*). *D*: image from the inverted scope of the recorded cell indicating fluorescence sampling locations (*red square*, soma; *blue square*, main dendritic trunk; *pink* and *green squares*, b1 and b2 dendritic branches).

tions in synchrony with the recorded electrical data (Fig. 4*A*, *red* and *black records*). Oscillations were also visible in the dendrites (Fig. 4*A*, *blue record*). The fluorescence was mostly extinguished by the addition of Cd^{2+}.

Cross-correlation analysis of the electrical and somatic fluorescence records from the cell depicted in Fig. 4*A* indicated a 12-msec lag with a peak frequency of ~7 Hz (Fig. 4*B*, *top*). Interestingly, the lag time matched the lag observed previously in high-speed Pf oscillation recordings (14). This is also supported by the power spectrum (Fig. 4*B*, *top*), with the somatic fluorescence signal showing a peak at 7 Hz (*red line*) that matched the 7-Hz peak in the electrical record (*black line*). This confirms that the oscillations observed in the fluorescence records were indeed calcium-mediated oscillations rather than background noise. Oscillations were visualized in the proximal dendrites of 14 OGB1/CHR-filled neurons. Figure 4*A* (*blue record*) demonstrates oscillations in one proximal dendrite that closely matched the simultaneously recorded electrical signal from the soma (*black record*). Similar oscillations were observed in dendritic branches (Fig. 4*C*, *green* and *pink records*). However, the two branches showed slightly different fluorescence activity compared with each other. Some oscillations were present in the *pink record* that were not present in the *green record* and vice versa. If the fluorescence activity of the two branches (*pink* and *green*) was mathematically summed, the resulting summation (Fig. 4*C*, *orange record*) closely matched that fluorescence record from the originating proximal dendrite (Fig. 4*A*, *blue record*).

Because we cannot directly observe calcium oscillations in distal dendritic compartments due to low levels of fluorescence, we carried out longer exposure wide-field imaging to confirm the presence of changes in calcium levels more distal in the dendritic tree. The low fluorescence in these distal dendrites required averaging eight individual ramps to increase the signal-noise ratio. We also used the Evolve 512 to increase the field of view. Thus the only limitation was the ability to sample as many dendrites, and as much of each dendrite's length, into a single focal plane. The composite single-wavelength OGB1 images were compared before and after the addition of AgA and CgTx (Fig. 5, *A* and *B*). Note that calcium levels increased along the length of the dendrite and were mostly uninterrupted. The addition of specific calcium-channel blockers eliminated the calcium changes. Our previous work on PPN oscillations showed that whereas oscillations were due to both P/Q-type and N-type voltage-gated calcium channels, the latter were permissive but not essential (21). To confirm this using calcium imaging, we repeated the wide-field experiments using only AgA. By leaving out CgTx, only P/Q-type channels were blocked, whereas N-type channels remained available. Wide-field imaging showed multiple dendrites fluorescing at the peak of the calcium transient (Fig. 5, *C* and *D*). The addition of AgA eliminated most but not all of the calcium fluorescence, with some fluorescence remaining around the soma. However, this fluorescence was only slightly above background levels, and we assume was mediated by N-type calcium channels.

Characterization of oscillation frequency in response to indicator presence. Oscillation frequencies were analyzed to determine whether the various calcium indicators induced any frequency changes. Although recordings using dye indicators showed slightly lower frequencies than control cells, statistical testing showed no significant differences between the oscillation frequency of each dye group and the control cells (Fura 2, 19 ± 2 Hz, $n = 20$; Bis Fura, 19 ± 2 Hz, $n = 20$; OGB1/CHR 20 ± 2 Hz, $n = 27$; CTRL, 23 ± 1 Hz, $n = 44$: ANOVA $F_{3,107} = 1.7$; $P = 0.18$). When the indicator groups were pooled and then divided by electrophysiological cell type, no significant differences were evident across cell types (indicator exposed cells: type I 19 ± 3 Hz, $n = 12$; type II 19 ± 2 Hz, $n = 27$; type III 20 ± 2 Hz, $n = 28$: ANOVA $F_{2,64} = 0.1$, $P = 0.9$), or each cell type compared with control cells (CTRL cells: type I 22 ± 3 Hz, $n = 14$, $P = 0.4$; type II 22 ± 1 Hz, $n = 19$, $P = 0.2$; type III 25 ± 1 Hz, $n = 11$, $P = 0.06$). Also, there was no significant difference between the three cell types in control cells (ANOVA $F_{41,2} = 1.2$, $P = 0.3$). An age-related analysis was not conducted because it was difficult to patch brainstem PPN neurons after 16 days due to the level of myelination.

DISCUSSION

This study showed that *1*) ratiometric analysis using three separate calcium probes revealed that calcium concentrations increased in PPN dendrites in parallel with the electrical ramp-induced signal (Fig. 2); *2*) high-speed imaging using ratiometric OGB1/CHR showed peaks in the calcium flux paralleling oscillations in the electrical signal (Fig. 3); and *3*) the mechanism behind both the ramp-induced electrical oscillations and visualized fluorescence oscillations was due to high threshold, voltage-dependent P/Q-type and N-type calcium channels (Figs. 2 and 3). We found that PPN neurons generated measureable calcium transients in response to depolarizing current ramps when action potential (APs) and synaptic inputs were blocked (Fig. 2). Calcium oscillations were present in both the recorded electrical signal and the fluorescence calcium signal. These oscillations were observed in both the soma and proximal dendrites. This is the first time that ramp-induced calcium oscillations have been described in the PPN using fluorescence calcium probes. Visualizing these oscillations allowed us to determine spatial variations in oscillations across the cell, whereas patch clamp recordings show only average oscillatory activity for the whole cell. On the basis of earlier studies in the Pf (14), we focused mainly on using both Fura 2 and Bis Fura as standards for analyzing calcium concentrations and transients. Bis Fura was used as well as Fura 2 despite the possibility that the higher affinity Fura 2 would low-pass-filter observed calcium dynamics. We then developed a ratiometric method using OGB1 to visualize calcium oscillations with high-speed imaging. These findings provide novel information for understanding PPN oscillatory activity.

Our resting somatic calcium concentrations were similar to resting concentrations reported in thalamic neurons (1, 3). Resting dendritic Fura 2 and Bis Fura calcium concentrations were slightly higher than concentrations reported in hippocampal neurons (45–133 nM) (3, 11, 34), whereas OGB1/CHR concentration was within the same range. Resting somatic concentrations were similar to those previously observed in the Pf, but resting dendritic concentrations were nearly twice those observed in the Pf (14). The higher dendritic concentration in PPN cells may be due to uncontrolled calcium activity in the dendrites. This may be due to ligand-gated calcium channels or to the opening of P/Q-type calcium channels located in den-

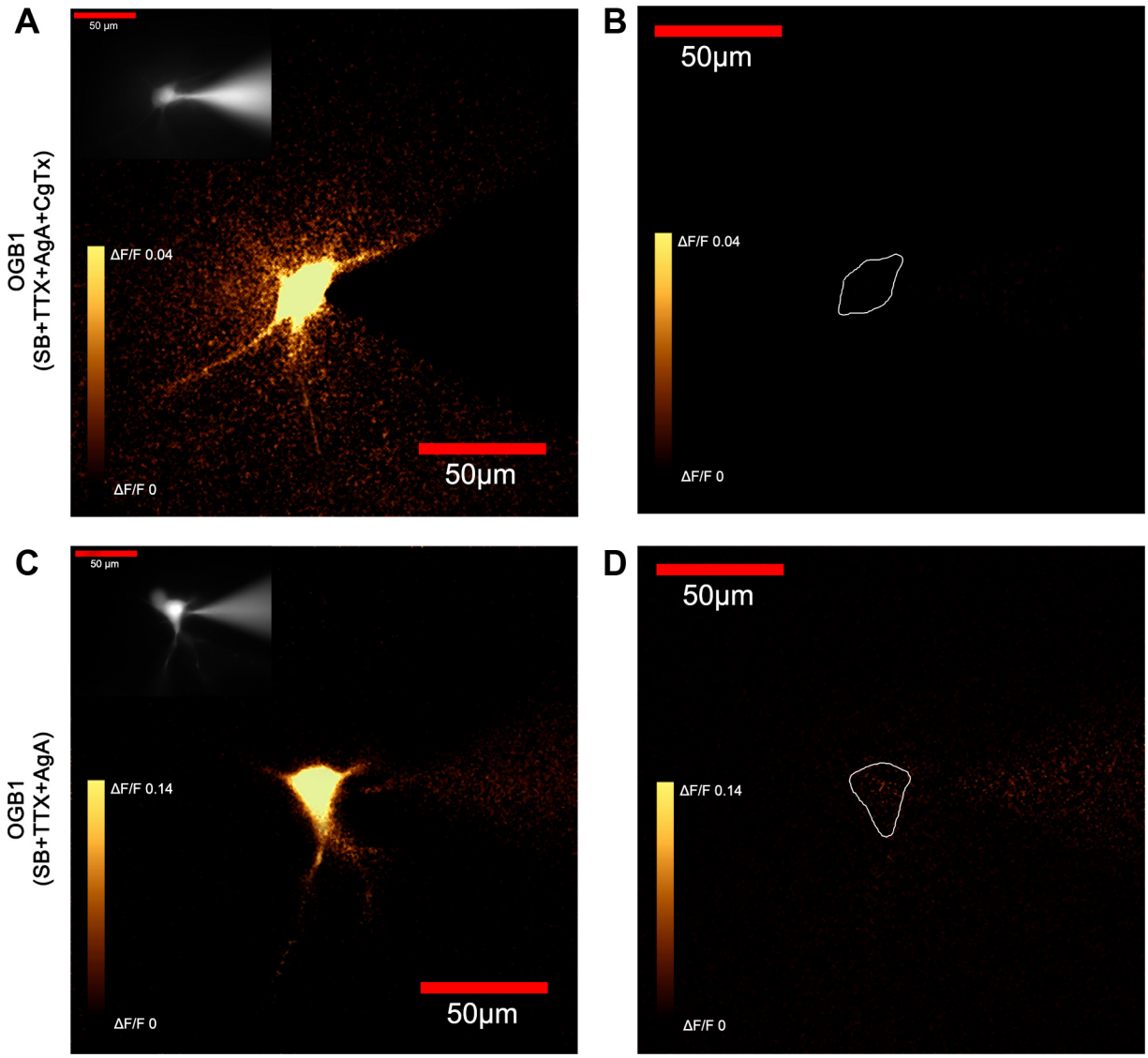

Fig. 5. Wide-field calcium imaging with OGB1. *A*: image from the peak of a calcium transient showing an increase in calcium levels. The increase was present continuously across the length of the dendrites. *Inset*: fluorescence zoom of the filled cell. *B*: AgA and CgTx eliminated all calcium transients. *C*: image from the peak of a calcium transient showing an increase in calcium levels. *Inset*: fluorescence zoom of the filled cell. *D*: AgA blocked P/Q-type channels and eliminated the majority of the fluorescence with some fluorescence remaining in the soma (N-type calcium channel-mediated). Note that the color map on the left of each image was scaled to match the peak fluorescence of each cell, and that *A* and *B* used different scales compared with *C* and *D*.

dritic compartments (28). Also, because no significant difference was found in the percent change between calcium indicators, we demonstrated that the OGB1/CHR indicator is valid for measuring calcium concentrations. Intracellular Fura 2 and Bis Fura indicator concentrations achieved in this study were capable of significantly changing the resting membrane potential, in keeping with their affinity for calcium, similar results were observed in Pf neurons (14). Interestingly, the OGB1/CHR probe showed no significant difference in membrane potential compared with control cells. This may be due to the lower indicator concentration used. This suggests the involvement of a calcium-dependent potassium current in the maintenance of resting membrane potential of PPN neurons. This study did not control extraneous potassium currents, thus it is possible for uncontrolled calcium-mediated potassium-channel activation to alter the membrane potential, which would explain the changes in resting membrane potential levels described here. However, no significant differences were observed between IV (current - voltage) curves of control cells and OGB1/CHR cells. Finally, no significant differences were found in the resting membrane potential between PPN neuronal subtypes, replicating previous results in the PPN (21), suggesting minimal interference with cellular properties by the indicators.

We showed an increase in calcium concentration in the dendrites that coincided with the peak of the calcium transient. The peak calcium concentration was within the range of calcium concentrations observed in the dendrites of cortical neurons during firing (383 nM) (2). However, this was mainly with Bis Fura. OGB1/CHR showed lower concentration levels. This was probably due to the lack of firing in PPN neurons exposed to synaptic blockers and TTX. More specifically, we

were recording membrane oscillatory activity, thus the calcium transients would be expected to be of lower amplitude than when APs are generated. It is possible that the depolarizing current ramps did not elicit the maximum possible amplitude calcium transients. Also, caution must be used when interpreting absolute calcium concentrations because the K_d value for each dye can vary widely depending on intracellular conditions such as temperature, ionic strength, and pH throughout PPN cellular compartments. We showed that the mechanism behind parallel ramp-induced electrical and fluorescence oscillations was due to high-threshold, voltage-dependent P/Q-type and N-type calcium channels. We found that PPN neurons produced measureable calcium transients in response to depolarizing current ramps even though all APs and synaptic inputs were blocked. The mechanism behind the generation of these oscillations has been previously shown to involve the opening of high-threshold, voltage-dependent P/Q-type and N-type calcium channels (20, 21). This set of experiments therefore replicated our previous results using only electrical recordings. The use of the nonspecific calcium channel blocker Cd^{2+}, or of the specific blockers AgA and CgTx, allowed us to eliminate both electrical oscillations and fluorescence calcium transients in PPN neurons.

The somatic area percent change of calcium influx showed no difference between electrophysiological cell types. However, the dendritic area percent change revealed that type II cells were significantly lower than type I or type III cells (with no difference between type I and type III cells). Type I and type III cells have previously been shown to have higher oscillation amplitudes (21), thus they should show higher calcium fluxes. The lack of significance in the somatic calcium fluxes can be attributed to the larger buffering capacity of the soma with its larger cytosolic volume. We also characterized the fluorescence calcium transients using synaptic blockers only, and omitting TTX. However, this occurred using only the OGB1/CHR indicator. Our previous experiments showed that TTX partially blocked gamma oscillations in PPN neurons during current steps (35). We tested the hypothesis that the area under the fluorescence curve would decrease when TTX was omitted, causing calcium channels to be inactivated by unclamped nearby synaptic neuronal activity as well as by recurrent overactivation of PPN dendritic compartments. This synaptic activity may include neurotransmitters that are not blocked by the synaptic blockers. There was no discernible difference in the calcium transient levels with and without TTX (Fig. 3). This may be due to differences between the recorded electrical signal and the fluorescence recording, because the electrical record is recording the sum of all electrical activity in the entire cell, which may include ionic activity other than calcium. Furthermore, many cells showed APs before and after calcium channel blockers when TTX was omitted while the fluorescence was eliminated. This suggests that the fluorescence signal was entirely due to calcium flux. However, sodium channel-mediated APs appear to be responsible for spreading the membrane depolarization needed to open high-threshold calcium channels presumably located in PPN dendrites, as suggested previously (21).

This study showed that high-speed imaging using OGB1/CHR can show that the peaks in fluorescence calcium flux parallel the oscillations in the electrical signal (Fig. 4). This is the first time that ramp-induced calcium oscillations have been described in the PPN using calcium-sensitive probes. Our previous experiments in the Pf showed that normal ratiometric imaging is insufficient to effectively record high-speed fluorescent calcium oscillations. Single-wavelength imaging with OGB1 proved more effective, but suffers from imaging problems inherent with the technique, such as variation between cells or surrounding optical density. To combine the advantages of ratiometric imaging with high-speed OGB1 imaging, we coinjected the noncalcium-sensitive CHR dye to act as a fluorescence benchmark. The unique long-stokes-shift of CHR allowed for simultaneous excitation and acquisition of OGB1 and CHR for continuous high-speed imaging. Combining this with ultrastable LED illumination created a powerful method for measuring fluorescent calcium oscillations. OGB1/CHR recordings showed that oscillations present in the somatic fluorescence records closely matched the electrical recordings, which indicated a summation of calcium signals arriving from the dendrites. The frequency and cross-correlation data in turn support the contention that the oscillations observed in the calcium signal were the same or similar frequency as those observed in the patch clamp record. Some delays in time were observed in the somatic fluorescence records, which may have been due to the larger cytosolic volume of the soma and kinetics of the dyes. This agrees with previous results reported in the Pf using OGB1 by itself (14). Finally, the oscillations were confirmed to be due to voltage-gated calcium channel activation, because the addition of Cd^{2+} eliminated oscillations in both the electrical and fluorescence recordings.

The oscillations present in the somatic fluorescence records closely matched the electrical patch clamp recordings, which indicated a summation of calcium signals arriving from the dendrites. This is supported by the results of summing fluorescence signals from different dendritic branches (Fig. 4). The summed signal was similar to a proximal dendritic signal. However, these oscillations did not precisely match oscillations evident in the electrical recordings or the somatic fluorescence recordings. Some oscillation peaks were missing or were present in some dendrites, but not others. This may be indicative of dendritic subdomains with some dendrites having greater influence over the total calcium signal. We know that these oscillations are dendritic in origin due to the high depolarizing voltage required for their induction, as previously described (21). This may also be due to the small sampling area where the fluorescence record was extracted from the image series. Oscillations may have occurred outside of this sampling region.

Although we were not able to directly visualize calcium oscillations in very distal dendritic compartments, we were able to visualize calcium increases using slower wide-field imaging with OGB1 (Fig. 5 and supplemental video; supplementary material for this article is available online at the Journal website). To visualize the contributions of each channel type to the calcium signal, we applied only AgA to block only P/Q-type channels, leaving N-type channels unblocked. Nearly all of the calcium fluorescence was blocked by AgA, suggesting that the N-type channels produced negligible amounts of fluorescence, only slightly above background levels. This indicates that the majority of the calcium flux was due to P/Q-type channels. This suggests that P/Q- and N-type voltage-gated calcium channels may play different roles in manifesting and modulating calcium oscillations.

To confirm that the calcium indicator was not affecting oscillation frequency, we compared average frequencies for each indicator. Although indicator-labeled cells appeared to have lower frequencies than control cells, statistical testing showed that this was not significant. The calcium indicator acts as a calcium buffer and slows calcium kinetics (13, 32, 34). We pooled the indicator-labeled neurons and compared the average cell type oscillation frequency and found no difference in frequency between cell types or compared with control cells. The most effective stimulation of the PPN for inducing long-lasting fast oscillations in thalamocortical cells and modulating the cortical electroencephalogram was three short trains at 300 Hz (37). Other work has proposed that high-frequency activation accounts for the temporal coherence of sensory perception in thalamocortical and cortical circuits (16, 25, 36). However, our previous results showed that type I, type II, and type III cells all fired at gamma band frequencies (21). The present results confirmed that all cell groups fired on average in the beta/gamma range with no difference in frequency between the three cell types. Changes in the PPN have been previously described during the developmental decrease in REM sleep (17). These include increases in cell firing rates from the beta range in early ages (9–12 days, before decreases in REM sleep) and later ages (13–16 days) to the gamma band range during the greatest drop in REM sleep after 16 days. However, difficulty in patching PPN neurons after 15 days complicates oscillation analysis in older animals and is outside the scope of this paper.

These findings demonstrate a useful methodology for studying high-speed oscillations without the use of multiphoton imaging systems. The wide-field imaging system allows for simultaneous acquisition from many areas without the timing delays due to laser scan time associated with visualizing large areas. However, this technique has limitations. A lower signal-to-noise ratio prevents recording in distal dendritic compartments. This may be achievable with multiphoton imaging, but currently cost and availability are limiting factors, whereas wide-field systems are more widely available. Further experiments may include bulk-loading experiments using AM (acetoxymethyl) calcium dyes. This may allow us to measure oscillations in many cells at once. We suggest that rather than participating in the temporal binding of sensory events, gamma band activity produced by the PPN may act to stabilize coherence related to arousal by unifying cell firing. This would then provide a stable activation state during waking and paradoxical sleep. Extensive work is still needed to verify this speculation, but calcium imaging may provide a useful methodology for analyzing the circuitry behind this activity.

ACKNOWLEDGMENTS

We thank Dr. Abdallah Hayar for his assistance with calcium signal analysis.

GRANTS

This work was supported by U.S. Public Health Service Grant R01-NS020246, and by core facilities of the Center for Translational Neuroscience Grants P20-GM103425 (to E.G.R.) and UL1-TR000039. In addition, F. J. Urbano was supported by FONCyT, Agencia Nacional de Promoción Científica y Tecnológica BID 1728 OC. AR; PICT 2008-2019 and PICT-2012-1769.

DISCLOSURES

No conflicts of interest, financial or otherwise, are declared by the author(s).

AUTHOR CONTRIBUTIONS

Author contributions: J.R.H., F.J.U., and E.G.-R. conception and design of research; J.R.H. and N.K. performed experiments; J.R.H., N.K., and F.J.U. analyzed data; J.R.H. and E.G.-R. interpreted results of experiments; J.R.H. and N.K. prepared figures; J.R.H., N.K., F.J.U., and E.G.-R. drafted manuscript; J.R.H., F.J.U., and E.G.-R. edited and revised manuscript; J.R.H., F.J.U., and E.G.-R. approved final version of manuscript.

REFERENCES

1. **Budde T, Sieg F, Braunewell KH, Gundelfinger ED, Pape HC.** Ca2+-induced Ca2+ release supports the relay mode of activity in thalamocortical cells. *Neuron* 26: 483–492, 2000.
2. **Cornelisse LN, van Elburg RA, Meredith RM, Yuste R, Mansvelder HD.** High speed two-photon imaging of calcium dynamics in dendritic spines: consequences for spine calcium kinetics and buffer capacity. *PLoS One* 2: e1073, 2007.
3. **Coulon P, Herr D, Kanyshkova T, Meuth P, Budde T, Pape HC.** Burst discharges in neurons of the thalamic reticular nucleus are shaped by calcium-induced calcium release. *Cell Calcium* 46: 333–346, 2009.
4. **Datta S, Patterson EH, Spoley EE.** Excitation of the pedunculopontine tegmental NMDA receptors induces wakefulness and cortical activation in the rat. *J Neurosci Res* 66: 109–116, 2001.
5. **Datta S, Siwek DF.** Single cell activity patterns of pedunculopontine tegmentum neurons across the sleep-wake cycle in the freely moving rats. *J Neurosci Res* 70: 611–621, 2002.
6. **Datta S, Spoley EE, Patterson EH.** Microinjection of glutamate into the pedunculopontine tegmentum induces REM sleep and wakefulness in the rat. *Am J Physiol Regul Integr Comp Physiol* 280: R752–R759, 2001.
7. **Eckhorn R, Bauer R, Jordan W, Brosch M, Kruse W, Munk M, Reitboeck HJ.** Coherent oscillations: a mechanism of feature linking in the visual cortex? Multiple electrode and correlation analyses in the cat. *Biol Cybern* 60: 121–130, 1988.
8. **Garcia-Rill E.** Reticular activating system. In: *The neuroscience of sleep.* Edited by Stickgold R, Walker M. Oxford, UK: Elsevier, 2009, p. 133–139.
9. **Garcia-Rill E, Heister DS, Ye M, Charlesworth A, Hayar A.** Electrical coupling: novel mechanism for sleep-wake control. *Sleep* 30: 1405–1414, 2007.
10. **Garcia-Rill E, Ye M, Heister D.** Novel mechanism for sleep-wake control: electrical coupling. *SRS Bull* 14: 8–10, 2008.
11. **Goldberg JH, Tamas G, Aronov D, Yuste R.** Calcium microdomains in aspiny dendrites. *Neuron* 40: 807–821, 2003.
12. **Gray CM, Singer W.** Stimulus-specific neuronal oscillations in orientation columns of cat visual cortex. *Proc Natl Acad Sci USA* 86: 1698–1702, 1989.
13. **Higley MJ, Sabatini BL.** Calcium signaling in dendritic spines. *Cold Spring Harb Perspect Biol* 4: a005686, 2012.
14. **Hyde J, Kezunovic N, Urbano FJ, Garcia-Rill E.** Visualization of fast calcium oscillations in the parafascicular nucleus. *Pflugers Arch* 465: 1327–1340, 2013.
15. **Iannuccelli E, Mompart F, Gellin J, Lahbib-Mansais Y, Yerle M, Boudier T.** NEMO: a tool for analyzing gene and chromosome territory distributions from 3D-FISH experiments. *Bioinformatics* 26: 696–697, 2010.
16. **Jones EG.** Calcium channels in higher-level brain function. *Proc Natl Acad Sci USA* 104: 17903–17904, 2007.
17. **Jouvet-Mounier D, Astic L, Lacote D.** Ontogenesis of the states of sleep in rat, cat, and guinea pig during the first postnatal month. *Dev Psychobiol* 2: 216–239, 1970.
18. **Jun K, Piedras-Renteria ES, Smith SM, Wheeler DB, Lee SB, Lee TG, Chin H, Adams ME, Scheller RH, Tsien RW, Shin HS.** Ablation of P/Q-type Ca(2+) channel currents, altered synaptic transmission, and progressive ataxia in mice lacking the alpha(1A)-subunit. *Proc Natl Acad Sci USA* 96: 15245–15250, 1999.
19. **Kao JP.** Practical aspects of measuring [Ca2+] with fluorescent indicators. *Methods Cell Biol* 40: 155–181, 1994.
20. **Kezunovic N, Hyde J, Simon C, Urbano FJ, Williams DK, Garcia-Rill E.** Gamma band activity in the developing parafascicular nucleus. *J Neurophysiol* 107: 772–784, 2012.
21. **Kezunovic N, Urbano FJ, Simon C, Hyde J, Smith K, Garcia-Rill E.** Mechanism behind gamma band activity in the pedunculopontine nucleus. *Eur J Neurosci* 34: 404–415, 2011.

22. **Leonard C, Llinas R.** Electrophysiology of mammalian pedunculopontine and laterodorsal tegmental neurons in vitro. In: *Brain Cholinergic Systems*, edited by Steriade M, Biesold D. New York: Oxford University Press, 1990.
23. **Llinas RR, Choi S, Urbano FJ, Shin HS.** Gamma-band deficiency and abnormal thalamocortical activity in P/Q-type channel mutant mice. *Proc Natl Acad Sci USA* 104: 17819–17824, 2007.
24. **Llinas RR, Pare D.** Of dreaming and wakefulness. *Neuroscience* 44: 421–435, 1991.
25. **Llinas R, Urbano FJ, Leznik E, Ramirez RR, van Marle HJ.** Rhythmic and dysrhythmic thalamocortical dynamics: GABA systems and the edge effect. *Trends Neurosci* 28: 325–333, 2005.
26. **Miura KR.** Bleach corrector. In: *EMBL Heidelberg*, http://cmci.embl.de/downloads/bleach_corrector [2013].
27. **Palva S, Monto S, Palva JM.** Graph properties of synchronized cortical networks during visual working memory maintenance. *Neuroimage* 49: 3257–3268, 2010.
28. **Pedroarena C, Llinas R.** Dendritic calcium conductances generate high-frequency oscillation in thalamocortical neurons. *Proc Natl Acad Sci USA* 94: 724–728, 1997.
29. **Phillips S, Takeda Y.** Greater frontal-parietal synchrony at low gamma-band frequencies for inefficient than efficient visual search in human EEG. *Int J Psychophysiol* 73: 350–354, 2009.
30. **Rasband W.** ImageJ. Bethesda, MD: National Institutes of Health, 1997–2004.
31. **Reese NB, Garcia-Rill E, Skinner RD.** The pedunculopontine nucleus–auditory input, arousal and pathophysiology. *Prog Neurobiol* 47: 105–133, 1995.
32. **Sabatini BL, Oertner TG, Svoboda K.** The life cycle of Ca(2+) ions in dendritic spines. *Neuron* 33: 439–452, 2002.
33. **Sakai K, el Mansari M, Jouvet M.** Inhibition by carbachol microinjections of presumptive cholinergic PGO-on neurons in freely moving cats. *Brain Res* 527: 213–223, 1990.
34. **Segal M.** Imaging of calcium variations in living dendritic spines of cultured rat hippocampal neurons. *J Physiol* 486, Pt 2: 283–295, 1995.
35. **Simon C, Kezunovic N, Ye M, Hyde J, Hayar A, Williams DK, Garcia-Rill E.** Gamma band unit activity and population responses in the pedunculopontine nucleus. *J Neurophysiol* 104: 463–474, 2010.
36. **Singer W.** Time as coding space? *Curr Opin Neurobiol* 9: 189–194, 1999.
37. **Steriade M, Dossi RC, Pare D, Oakson G.** Fast oscillations (20–40 Hz) in thalamocortical systems and their potentiation by mesopontine cholinergic nuclei in the cat. *Proc Natl Acad Sci USA* 88: 4396–4400, 1991.
38. **Steriade M, McCarley RW.** *Brainstem control of wakefulness and sleep.* New York: Plenum, 1990.
39. **Steriade M, Pare D, Datta S, Oakson G, Curro Dossi R.** Different cellular types in mesopontine cholinergic nuclei related to ponto-geniculo-occipital waves. *J Neurosci* 10: 2560–2579, 1990.
40. **Takahashi A, Camacho P, Lechleiter JD, Herman B.** Measurement of intracellular calcium. *Physiol Rev* 79: 1089–1125, 1999.
41. **Takakusaki K, Kitai ST.** Ionic mechanisms involved in the spontaneous firing of tegmental pedunculopontine nucleus neurons of the rat. *Neuroscience* 78: 771–794, 1997.
42. **Thevenaz P, Ruttimann UE, Unser M.** A pyramid approach to subpixel registration based on intensity. *IEEE Trans Image Process* 7: 27–41, 1998.
43. **Voss U, Holzmann R, Tuin I, Hobson JA.** Lucid dreaming: a state of consciousness with features of both waking and non-lucid dreaming. *Sleep* 32: 1191–1200, 2009.
44. **Wang HL, Morales M.** Pedunculopontine and laterodorsal tegmental nuclei contain distinct populations of cholinergic, glutamatergic and GABAergic neurons in the rat. *Eur J Neurosci* 29: 340–358, 2009.
45. **Ye M, Hayar A, Strotman B, Garcia-Rill E.** Cholinergic modulation of fast inhibitory and excitatory transmission to pedunculopontine thalamic projecting neurons. *J Neurophysiol* 103: 2417–2432, 2010.